Lawrence Berkeley Laboratory
UNIVERSITY OF CALIFORNIA

Materials & Molecular Research Division

Submitted to the Journal of Applied Physics

TEM AND RBS STUDIES OF SINGLE AND DOUBLE DISCRETE BURIED DAMAGE LAYERS IN P^+ IMPLANTED Si ON SUBSEQUENT LASER ANNEALING

D. K. Sadana, M. Strathman, J. Washburn and G. R. Booker

January 1980

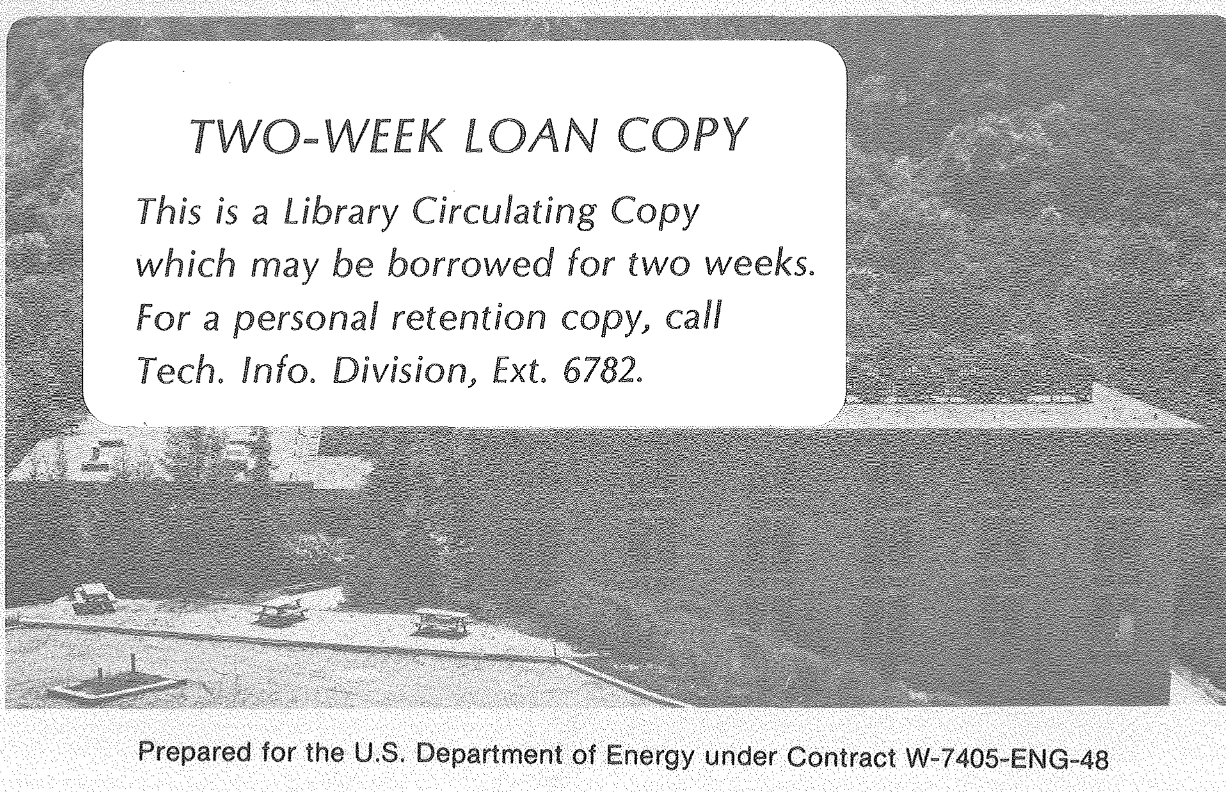

Prepared for the U.S. Department of Energy under Contract W-7405-ENG-48

LBL-10625

TEM AND RBS STUDIES OF SINGLE AND DOUBLE DISCRETE BURIED DAMAGE LAYERS IN P+ IMPLANTED Si ON SUBSEQUENT LASER ANNEALING

D.K. Sadana, M. Strathman, J. Washburn
Lawrence Berkeley Laboratory
University of California
Berkeley, California

G.R. Booker
Department of Metallurgy
University of Oxford, Oxford, England

ABSTRACT

This work is aimed at studying the regrowth behaviour of single and double buried damage layers on subsequent laser annealing of P^+ implanted Si, implanted at 120 keV to doses of $5 \times 10^{14}/cm^2$ and $7.5 \times 10^{15}/cm^2$, respectively. A Q-switched ruby laser operating at a wavelength of 0.695μm was used for the annealing. 90° cross sectional TEM and MeV He^+ channelling spectroscopy were used to examine the damage structures and their depth distributions. At 0.9 J/cm^2, TEM results showed that the single buried damage layer regrew into two discrete damage layers. At 2.0 J/cm^2, TEM results showed that the first layer in the double buried damage layers type structures either completely annealout out, leaving a partially annealed second layer consisting of damage clusters or had dislocations in the first damage layer region that extended from the surface and were in direct contact with the deeper lying second layer of damage clusters. The MeV He^+ channelling spectra for the above samples were in agreement with the TEM results.

INTRODUCTION

This work is a continuation of our previous studies on the regrowth behaviour of different types of implantation induced damage structures (1-3). These studies as well as the results of the earlier workers (4-7) indicate that the subsequent high power nano seconds laser irradiation causes short-term surface melting. For a given laser energy, the depth of the molten region was found to depend on the initial damage structures and its distribution in the irradiated material (1-3). The defects morphology in the regrown region depended critically on the depth of the molten region relative to the depth of the initial damage region (1-3, 8-10). In the present study, the regrowth behaviour of a single buried damage layer and two different types of double buried damage layers on subsequent laser annealing has been investigated. The samples with the latter type damage distributions were obtained from the implanted regions of the wafer that showed colour bands at the implanted surface. The colour bands often appear at the surface of a wafer, implanted at a high dose rate because of the non-uniform beam heating effects during the implantation. As a result, the optical interference between light reflected from the surface and from the variable depth of the sub-surface interface at which the refractive index changes gives rise to colour effect (11).

In the present experiments '90° cross-sectional TEM' and MeV He^+ channelling spectroscopy were used to obtain damage-depth distributions before and after the annealing. The nature of the damage was further revealed by 'plan' view TEM specimens. There was a good qualitative correlation between the results obtained from TEM and channelling measurements.

EXPERIEMENTAL

a. Implanation P-type 17 ohm-cm (111) Si wafers were implanted in a non-channelling direction with 120KeV P+ ions to doses of $5 \times 10^{14}/cm^2$ and $7.5 \times 10^{15}/cm^2$, respectively. For $7.5 \times 10^{15}/cm^2$ implant, the dose rate was ~$0.8 mA/cm^2/sec$ and the implantation temperature was estimated to have increased to 400°C at the end of the implantation cycle.

b. Laser A Q-switched ruby laser operating at a wavelength of 0.695 μm was used. The laser energies of either ~$0.9\ J/cm^2$ or ~$2.0\ J/cm^2$ were used. The pulse length for all the specimens was ~50 n sec.

c. TEM The preparation technique for both '90° cross- sectional' and 'plan' view specimens has already been described in the earlier publication (1). For all the 'cross-sectional' specimens, the bright field strong beam diffraction contrast method was used. The specimens were tilted to a two beam condition for a 220 type reflection.

d. RBS/channelling A 1.6 Mev He+ particle beam was accelerated in a Van de Graff generator and was collimated to <1 mm spot size. The back scattered particles were detected by a Si surface barrier type detector at an angle of170° with respect to the incident beam. For current integration, a magnetic Faraday cup arrangement was used (12).

RESULTS

a. Single Buried Amorphous Layer For the wafers implanted to a dose of $5 \times 10^{14}/cm^2$, the TEM 'cross-section' micrograph showed a buried amorphous layer 'K' (Fig. 1a). The region between the surface and the top edge of the damage layer 'K' had sparsely distributed clusters (for TEM data see Table I). The channelling results also showed peaks 'E' and 'F', indicating the presence of a buried damage layer under a heavily damaged surface region (Fig. 2.)

After the specimen has been laser annealed at 0.9 J/cm^2, the TEM micrograph showed two discrete damage layers 'L' and 'Z' in a single crystal material (Fig. 1b). The TEM data for these layers is given in Table 1. Layer 'L' contained small dislocation loops and layer 'Z' contained a high density of damage clusters. The channelling results showed three peaks, 'G_1', 'G_2' and 'G_3', respectively. Peak 'G_3' corresponded to the single crystal surface peak. Peaks 'G_2' and 'G_3' (Fig. 2) showed the presence of two discrete damaged regions. The scattering yield values indicated the surface to be damaged and the deeper damage layer to have more disorder as compared to that present in the shallower layer. This was in agreement with the TEM results.

b. Double Buried Damage Layers (Green Band) For the wafers implanted to a dose of $7.5 \times 10^{15}/cm^2$, and showing a mutlicoloured band at the implanted surface, the TEM micrograph from the 'green' region showed two discrete buried damage layers 'P' and 'Q' in a single crystal material (Fig. 3a). The TEM data is given in Table I. The channelling spectra showed three discrete peaks, 'C_1', 'C_2' and 'C_3', respectively. Peak 'C_1' corresponded to the surface peak in single crystal material

(Fig. 4). Peaks 'C_2' and 'C_3' showed the presence of two discrete buried damage layers. The scattering yield values indicated that the disorder in the shallower layer was more than that in the deeper layer. These results were in agreement with the TEM results.

On subesequent annealing at 2.0 J/cm^2, the TEM micrograph showed that the shallower damage layer 'P' in the unannealed specimen was no longer present; however, the deeper layer 'Q' was still present but was less in evidence (layer 'R' in Fig. 3b; for TEM data, see Table 1). The channelling results (Fig. 4) gave a single crystal spectrum but showed an increased dechannelling in the deeper regions.

c. <u>Double Buried Damage Layers (Blue-Green Band)</u> The TEM micrograph from the 'blue-green' region of the previous wafer again showed two discrete buried damage layers 'S' and 'T' (Fig. 5a) but the depth distribution of the damage here was different as compared to that in the previous 'green' band specimen. The TEM data is given in Table I. The channelling spectra (Fig. 6) again showed three discrete peaks, 'D_1','D_2' and 'D_3', respectively. The scattering yield values of the peaks indicated that the surface region was single crystal but was damaged. This was followed by two discrete damage regions.

On subsequent annealing at 2.0 J/cm^2, the TEM micrograph showed that the shallower damage layer 'S' in the unannealed specimen regrew to form a layer of dislocations, 'U', (Fig. 5b) that was in direct contact with a dense layer of damage clusters, 'V', and the dislocations extended to the surface. (TEM data, see Table I). The channelling spectra showed two peaks 'D'and '$D^{\prime\prime}$' (Fig. 6). Peak 'D' corresponded to the surface peak in single crystal material. However, peak '$D^{\prime\prime}$' indicated that a discrete damage region was present deeper into the material. The scattering yield values indicated relatively less disorder in the damage layer. This was in agreement with the TEM results.

DISCUSSION

The mechanism of formation of two discrete layers of damage on subsequent laser annealing of a single buried amorphous layer is not yet clear. If melting has occurred, the subsequently cooled molten region would have contained dislocations nucleating from the underlying damage that would extend to the surface as observed earlier (1-3, 8,9) Since this did not occur, it has been conjectured that the regrowth occurred in a quasi-molten state. The energy absorption at the surface is expected to be less as compared to that at the upper edge of the buried amorphous layer (13). This differential absorption of laser energy could create a buried quasi-molten region at the top edges of damage layer 'K' (Fig. 1a). The subsequent cooling of the quasi-molten layer could form embryonic small dislocation loops. However, the presence of dislocations originating from the deeper layer of damage clustsers and extenting up to the surface both for the above specimen (3) and the 'blue-green' specimen on subsequent laser annealing at higher energies indicated that the melting occurred during the annealing and that the depth of the molten zone was either less or nearly equal to the width of the total damaged region in the as implanted specimen. The width of the molten zone (Table I) obtained here is in disagreement with that calculated by earlier workers both theroetically and experimentally. This apparent discrepancy could be attributed to significantly different average absorption coefficients of different coloured regions at the surface and also to the unique damage distribution present underneath these colour bands that could affect the energy coupling in the surface region.

CONCLUSIONS

1. The regrowth of the damage in P^+ implanted Si on subsequent pulsed laser annealing can occur either via quasi-molten phase epitaxy or liquid phase epitaxy, depending on the laser energy used and the depth distribution of damage present.

2. There is a good qualitative correlation between the cross-sectional TEM and MeV He^+ channelling results. The discrete damaged region in TEM micrographs appear as discrete damage peaks in the channelling spectra.

ACKNOWLEDGEMENTS

The authors would like to thank Dr. J. Stephens of AERE, Harwell (England) for implanting the Si wafers; Dr. D. Milam of Lawrence Livermore Laboratory, Berkeley (USA), for laser annealing the specimens. Finally we acknowledge the financial support of the Office of Basic Research of the Department of Energy through the Materials and Molecular Research Division, and the Department of Instrument Techniques of Lawrence Berkeley Laboratory, Berkeley (USA).

REFERENCES

1. D.K. Sadana, M.C. Wilson and G.R. Booker, J. Microscopy, 118, (1980).

2. D.K. Sadana, M.C. Wilson, G.R. Booker and J. Washburn, Extended Abstracts, 79 (2), E.S.C. Mtg. (Los Angeles, Oct. 1979), p. 1293.

3. D.K. Sadana, M.C. Wilson, G.R. Booker and J. Washburn, J. Electrochem. Soc., (in Press).

4. G.K. Celler, J.M. Poate and L.C. Kimerling, App. Phys. Lett., 32, 464 (1978).

5. C.W. White, W.H. Christie, B.R. Appleton, S.R. Wilson, P.P. Pronko and C.W. Magee, App. Phys. Lett., 33, 662 (1978).

6. P. Baeri, S.V. Campisano, G. Foti and E. Rimmi, Phys. Rev. Lett., 41, 1246 (1978).

7. D.H. Auston, C.M. Surko, T.N.C. Venkatesan, R.E. Slusher and J.A. Golovchenko, App. Phys. Lett., 33, 437 (1978).

8. A.G. Cullis, M.C. Webber, J.M. Poate and N.G. Chew, J. Microscopy, 118 (1980).

9. A.C. Cullis and H.C. Weber, Proc. E.C.S. Mtg (Los Angeles, Oct 1979).

10. J. Narayan, App. Phys. Lett., 36, 312 (1978).

11. T.E. Seidel, G.A. Pasteur and J.C. Tsai, App. Phys. Lett., 29, 648 (1976).

12. M. Strathman and M. Green, to be published.

13. B.G. Bagley and M.S. Chen in Laser Solid Interactions and Laser Processing--1978, ed. S.D. Ferris, H.J. Learny and J.M. Poate. Am. Inst. Phys., New York (1979), p. 97.

FIGURE CAPTIONS

Fig. 1. TEM 90° cross-sectional micrographs for $Np^+ = 5\times10^{14}/cm^2$, E=120 keV, T_i=RT. a) Unannealed b) L.A., $0.9 J/cm^2$.

Fig. 2. 1.6 MeV He^+ channelling spectra for UA and LA specimens.

Fig. 3. TEM 90° cross-sectional micrographs for $Np^+ = 7.5\times10^{15}/cm^2$, E_i=120 keV, Green Band.

Fig. 4. 1.6 MeV He^+ channelling spectra for UA and LA specimens.

Fig. 5. TEM 90° cross-sectional micrographs for $Np^+ = 7.5\times10^{15}/cm^2$, E_i=120 keV, Blue-Green Band.

Fig. 6. 1.6 MeV He^+ channelling spectra for UA and LA specimens.

Table I

Dose	Shallow Layer				Deep Layer			
	Unannealed		Laser annealed		Unannealed		Laser annealed	
	Width*	Mean Depth*	Width*	Mean Depth*	Width*	Mean Depth*	Width*	Mean Depth*
5×10^{14}	1350	1100	400(L)	1070(L)	---	---	---	---
			400(Z)	1600(Z)				
7.5×10^{15} (Green)	870	750	550	1560	---	---	400	2400
7.5×10^{15} (Blue-Green)	530	930	1730	870	470	1800	930	2200

*The measurement unit is in Å.

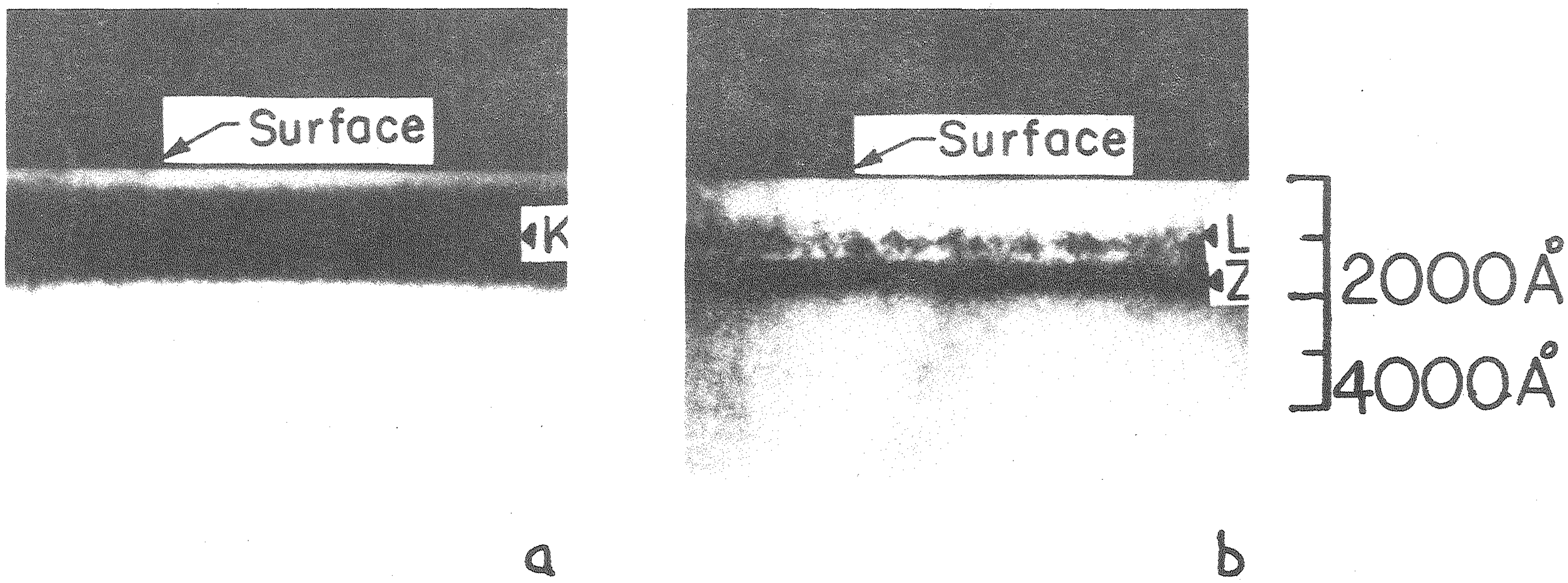

Figure 1

XBB801 312

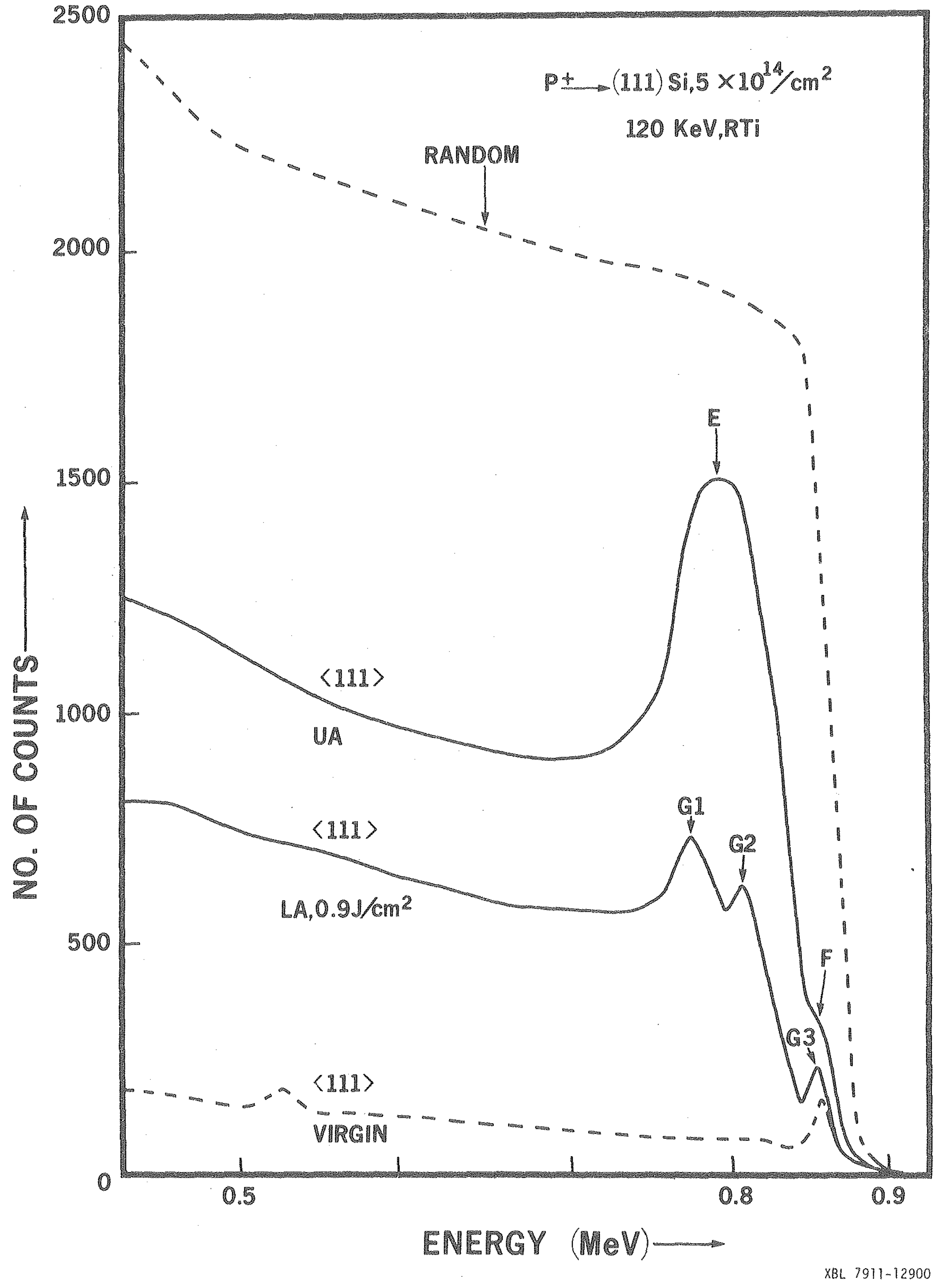
2500
2000
1500
1000
500
0
0.5
0.8
0.9
NO. OF COUNTS
ENERGY (MeV)
P+ → (111) Si,5 ×10^14/cm^2
120 KeV,RTi
RANDOM
E
⟨111⟩
UA
⟨111⟩
G1
G2
LA,0.9J/cm^2
F
G3
⟨111⟩
VIRGIN
XBL 7911-12900

Figure 2

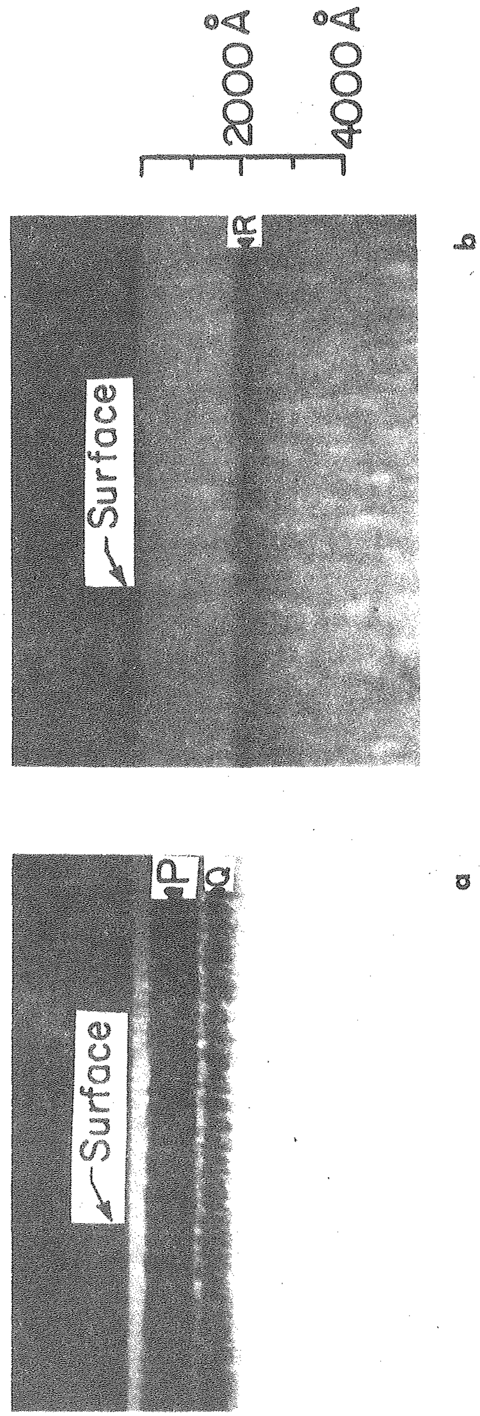

Figure 3

XBB790-15682

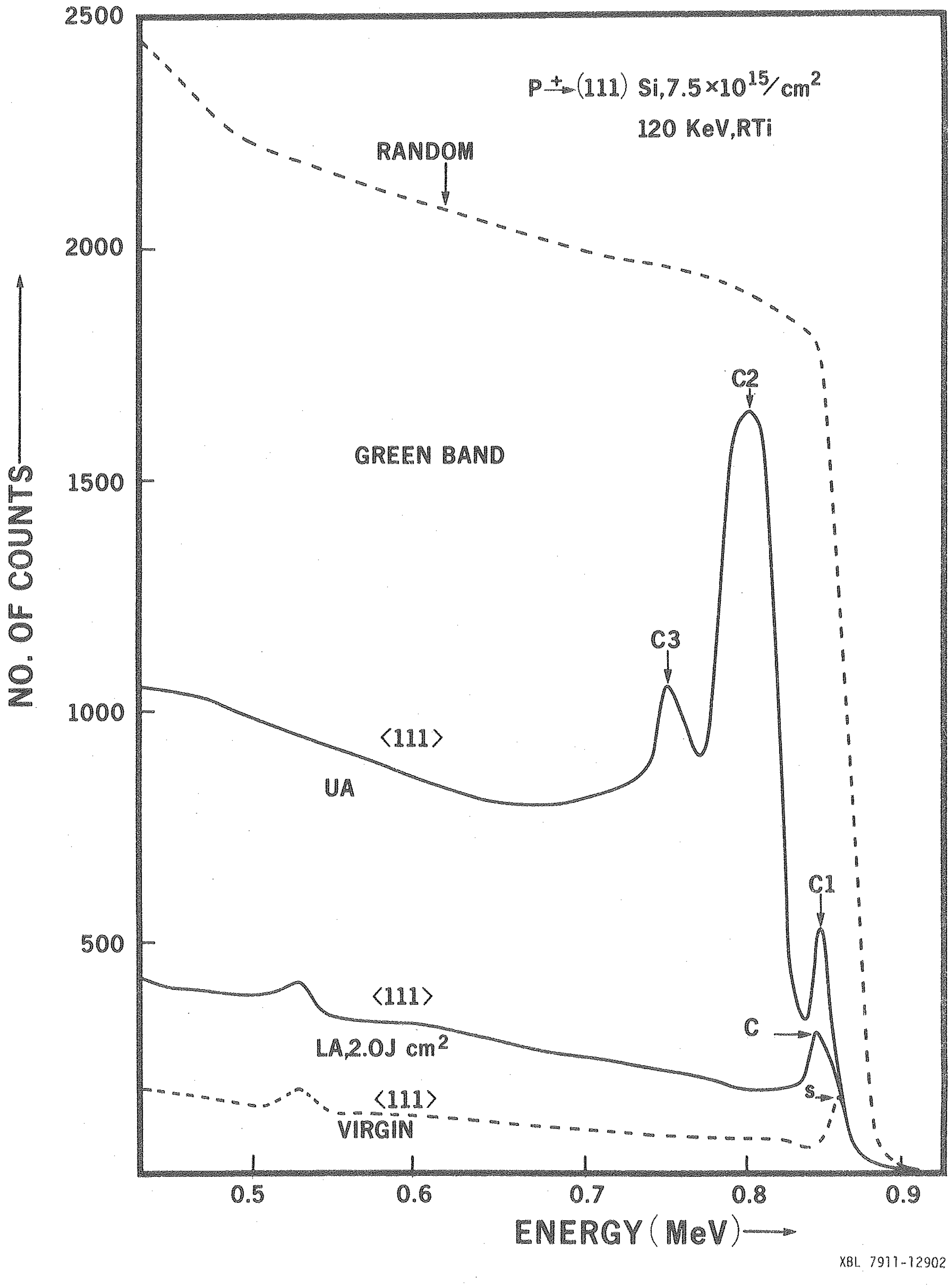
2500
2000
1500
1000
500
NO. OF COUNTS
P⁺→(111) Si,7.5×10¹⁵/cm²
120 KeV,RTi
RANDOM
GREEN BAND
C2
C3
C1
⟨111⟩
UA
⟨111⟩
LA,2.0J cm²
C
s
⟨111⟩
VIRGIN
0.5
0.6
0.7
0.8
0.9
ENERGY (MeV)
XBL 7911-12902

Figure 4

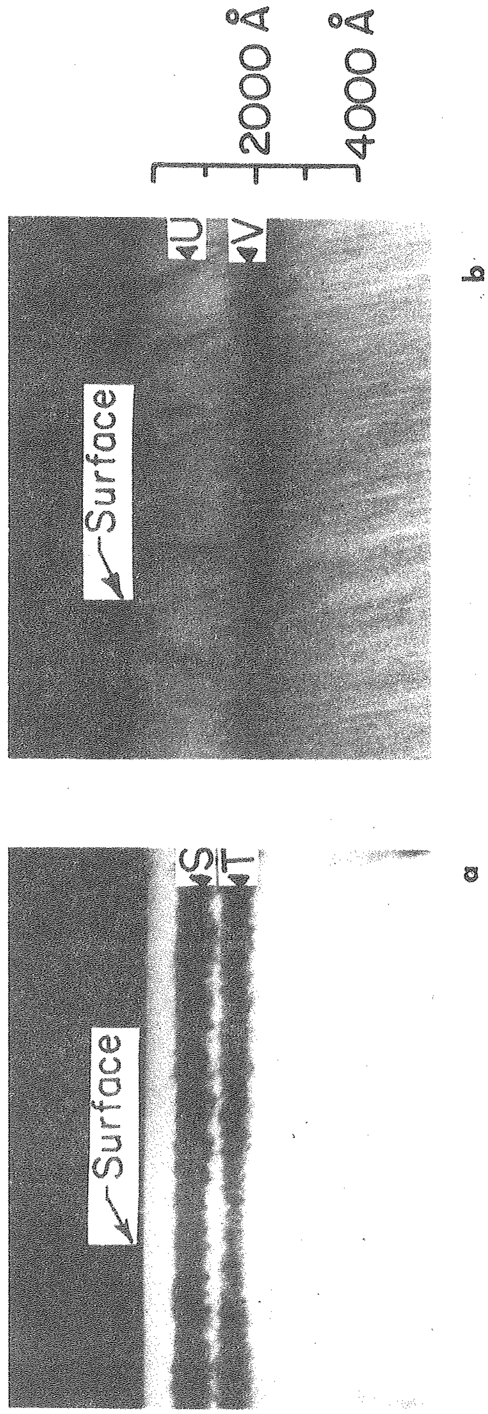

XBB790-15683

Figure 5

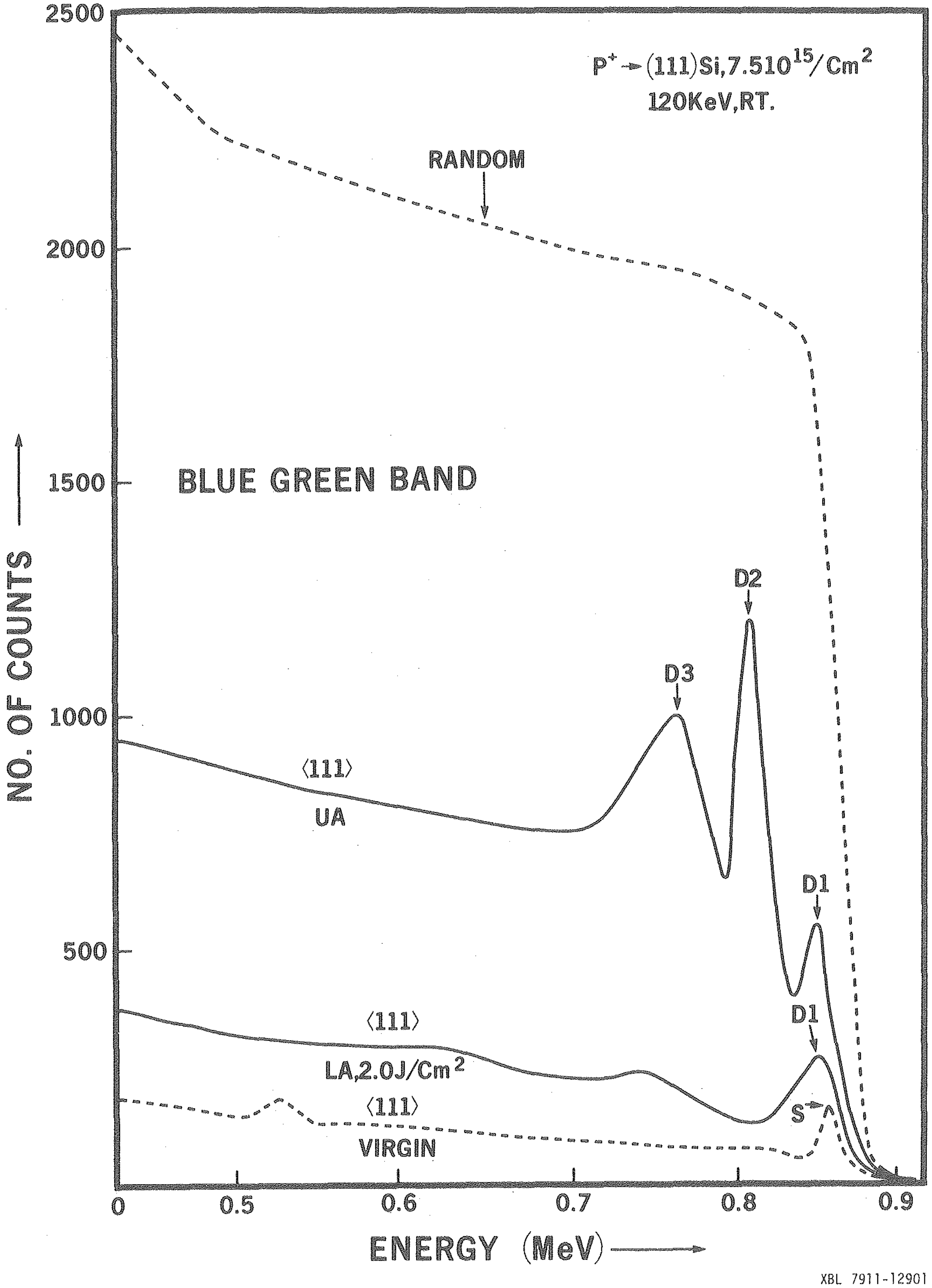
P⁺ → (111)Si,7.5 10^15/Cm^2
120KeV,RT.
RANDOM
BLUE GREEN BAND
D2
D3
D1
⟨111⟩
UA
D1
⟨111⟩
LA,2.0J/Cm^2
⟨111⟩
S
VIRGIN
2500
2000
1500
1000
500
0
0.5
0.6
0.7
0.8
0.9
NO. OF COUNTS
ENERGY (MeV)
XBL 7911-12901

Figure 6